RESEARCH ARTICLE

NANO · MICRO small
www.small-journal.com

Delicate Regulation of Central Substituents Boosts Organic Photovoltaic Performance of Dimeric Acceptors

Xinyuan Jia, Yu Li, Xiangjian Cao, Xingqi Bi, Wenkai Zhao, Zhaoyang Yao, Guankui Long, Bin Kan, Yaxiao Guo,* Chenxi Li, Xiangjian Wan, and Yongsheng Chen**

Dimeric acceptors are expected to satisfy both excellent power conversion efficiency (PCE) and operational stability of organic solar cells (OSCs). However, comparing to highly planar and symmetrical monomer-like acceptors, the quite different steric/spatial configurations of dimeric acceptors affect device outcomes greatly. Herein, on basis of the same dimeric molecular platform that constructed by bridging central units of two monomer-like acceptor, diverse substituents (—OCH_3 for D1, —CH_3 for D2, and —CF_3 for D3) are grafted on central units to regulate the three dimensions (3D) geometries of dimeric acceptors delicately. A systematic investigation reveals the substituent-dependent variation of energy level, absorption, and molecular packing behavior. Consequently, D2 acceptor, characteristic of more favorable configuration, affords a superior film morphology and charge transfer/transport dynamics in resulting OSCs, thus yielding an excellent PCE of 17.50% along with a good long-term stability. This work manifests the crucially important role of central substituents in constructing high-performance dimeric acceptors.

1. Introduction

Organic solar cells (OSCs), characteristic of amazing merits in light acquisition ability, device flexibility, low cost, and tunable transparency, have attracted enormous research and industrial attentions.[1–6] In recent years, the power conversion efficiency (PCE) of OSCs has stepped over 20%, mainly profiting from the advances in photovoltaic materials and morphology optimization of photoactive layers.[7–12] With the aim of meeting requirements for industrialization, plenty of efforts have been devoted to overcoming the currently unsatisfied long-term operational stability of OSCs.[13] Among them, enlarging molecular size of small molecular acceptors (SMAs) to limit molecular diffusion in blended films, such as exploring giant acceptors of dimer, trimer, and polymer, has been regarded as a feasible but quite effective strategy to improve device stability.[14–18] At present, nearly all the high-performance giant acceptors are designed by directly coupling two electron-withdrawing terminals of Y-series acceptors.[19–24] However, this constructing pathway will bring about some inherent flaws. 1) Insufficient terminal packing. The coupling reaction that occurs mainly on terminal units will decrease the number of free terminals, thus weakening intermolecular packings of giant acceptors by damaging π–π stacking of planar terminals.[25–27] Given its important role of terminal stacking in constructing desirable 3D packing networks, the efficient charge transfer/transport in OSCs may be inhibited to some extent. 2) Less halogen on conjugated backbones. The conventional pathway to build giant acceptors will inevitably occupy the halogenated active sites on terminals.[28,29] The lack of halogens on molecular backbones could also damage the halogen bonds between adjacent molecules, which is unfavorable for efficient molecular packing and charge migration.[30–32] 3) Spatial isomerization. Currently, possibly the only high-performance terminal units to construct SMAs are 1,1-dicyanomethylene-3-indanone (IC) and its halides.[33] In order to conduct the terminal coupling reaction successfully, it is quite essential to perform prebrominating on IC group. However, due to the lack of reactive selectivity, a mixture of two brominated isomers will be yielded. This usually results in purification dilemma due to their highly similar polarity, furthermore, gives rise to decreased PCEs if ignoring the problem of isomerization.[34]

X. Jia, Y. Li, X. Cao, X. Bi, Z. Yao, C. Li, X. Wan, Y. Chen
State Key Laboratory and Institute of Elemento-Organic Chemistry
The Centre of Nanoscale Science and Technology and Key Laboratory of Functional Polymer Materials
Renewable Energy Conversion and Storage Center (RECAST)
College of Chemistry
Nankai University
Tianjin 300071, China
E-mail: zyao@nankai.edu.cn; yschen99@nankai.edu.cn

W. Zhao, G. Long, B. Kan
School of Materials Science and Engineering
National Institute for Advanced Materials
Nankai University
Tianjin 300350, China

Y. Guo
State Key Laboratory of Separation Membranes and Membrane Processes and Key Laboratory of Hollow Fiber Membrane Materials and Membrane Processes (MOE)
School of Chemistry
Tiangong University
Tianjin 300387, China
E-mail: yaxiaoguo@tiangong.edu.cn

The ORCID identification number(s) for the author(s) of this article can be found under https://doi.org/10.1002/smll.202405925

DOI: 10.1002/smll.202405925

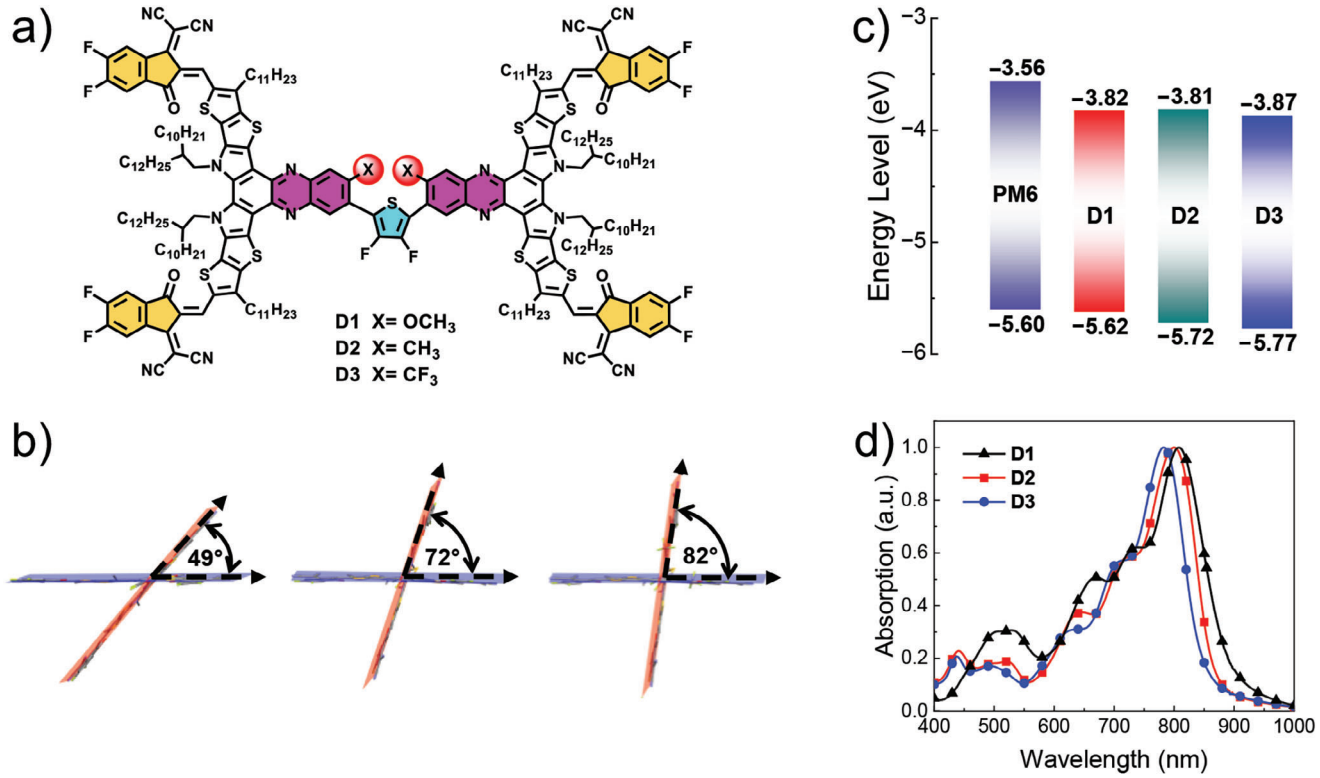

Figure 1. a) The chemical structures of D1, D2, and D3. b) The illustration of dihedral angle between two wings in D1, D2, and D3, respectively. c) The energy levels of PM6 and D1, D2, and D3. d) Normalized absorption profiles of D1, D2, and D3 based neat films, respectively.

Based on above analysis, a new type of dimeric acceptors has been developed by extending linear molecular skeletons toward three dimensions (3D).[35,36] These dimeric acceptors could be easily constructed through the direct connection of central units between two CH-series acceptors, rather than the terminal units coupling that widely applied by numerous conventional dimeric acceptors.[37–41] Theoretically, at the single-molecular level, such a 3D molecule could yield enlarged absorption coefficient and decreased reorganization energy benefiting from its significantly extended conjugated plane, when comparing to their monomer counterparts. Moreover, at the aggregation level, 3D acceptors that featuring with a suitably twisted molecular plane or desired steric hindrance may prefer to generate a more robust stacking network, which was driven by both the strengthened π–π stacking and noncovalent bonds.[29] This is conductive to enhancing the morphological stability of D/A blended active layers, thus contributing to highly stable and efficient OSCs.[42]

Bear these considerations in mind, three dimeric acceptors were constructed by means of directly coupling central units of two CH-series small molecular acceptors. All the three newly designed 3D acceptors (D1, D2, and D3) have the same conjugated backbones and four fluorine-substituted terminals (**Figure** 1a). Moreover, substituents with quite different electrical properties (—OCH_3 for D1, —CH_3 for D2, and —CF_3 for D3) were grafted on phenazine units, regulating conformations of acceptors delicately and further optimizing their molecular stacking, crystallinity and charge transfer/transport behaviors in resulting films. As a consequence, a remarkable PCE of 17.50% could be afforded by D2-based binary OSCs along with an open-circuit voltage (V_{OC}) of 0.926 V, short-circuit current density (J_{SC}) of 25.02 mA cm^2, and fill factor (FF) of 75.50%. Meanwhile, a good long-term stability could also be achieved by D2-based OSCs. Our work manifests the crucially important role of central substituents in structure optimization of dimeric acceptors and provides a feasible strategy to improve performance of dimeric acceptor-based OSCs further.

2. Results and Discussions

The synthetic routes to dimeric acceptors of D1, D2, and D3 were described in Scheme S1 of the Supporting Information. As unveiled by density functional theory (DFT) calculations, the dihedral angle between two conjugated planes of CH-series SMAs increases gradually from D1 to D3 (Figure 1b; Figure S1, Supporting Information). The central substituent of methoxy group (—OCH_3) on D1 is expected to form the noncovalently conformational lock through O–S interactions,[43,44] which should account for its smallest dihedral angle. When replacing —OCH_3 group with methyl (—CH_3), the dihedral angle in D2 enlarges significantly, and further is inclined to become more uneven in D3 due to the increased steric hindrance of trifluoromethyl (—CF_3) group. The successful regulation of molecular geometries highlights the effectiveness of central substituents in configuration control, which may also affect their resulting photovoltaic performance greatly. Then, the DFT calculated energy levels and frontier molecular orbital distributions were displayed in Figure S2 of the Supporting Information.[45] Both the highest occupied molecular orbital (HOMO) and lowest unoccupied molecular

orbital (LUMO) energy levels gradually downshift as the electron donating ability of central substituents decreasing from D1 to D3. It is worth noting that a relatively larger change on HOMOs (by ≈150 meV) than those of LUMOs (by ≈80 meV) can be observed, thus giving rise to the stepwise enlarged bandgaps from D1 to D3. Because of the strong electron-donating feature of central donors, HOMOs fully delocalize on the skeleton of S,N-heterocycle for all the three dimeric acceptors, while LUMOs mainly distribute along the whole molecular backbones with the maximum probability on fluorinated 2-(3-oxo-2,3-dihydro-1H-inden-1-ylidene)malononitrile terminals. The extensive spatial overlap between HOMOs and LUMOs is expected to enhance intramolecular charge transfer of acceptors and further render near-infrared absorptions. The experimental HOMOs and LUMOs of D1, D2, and D3 can also be roughly estimated by performing cyclic voltammetry (CV) measurements (Figure S3, Supporting Information). As illustrated in Figure 1c, the experimental HOMOs are −5.62, −5.72, and −5.77 eV for D1, D2, and D3, respectively. While the LUMOs could be estimated as −3.82 eV for D1, −3.81 eV for D2, and −3.87 eV for D3. The gradually downshifted HOMOs will afford a larger driving force for exciton dissociation in theory and are favor of more efficient charge generation in resulting OSCs. Note that the relative layout of HOMOs and LUMOs of D1, D2, and D3 including their corresponding bandgaps keeps a good accordance with the results predicted by DFT calculations (Table S1, Supporting Information).

As presented in Figure 1d and Figure S4 (Supporting Information), the absorption spectra of D1, D2, and D3 in chloroform solutions and spinning coating solid films were recorded to demonstrate their light-harvesting abilities. In dilute chloroform solutions, the maximum absorption peaks of D1, D2, and D3 locate at 755, 750, and 733 nm, respectively. Moreover, the similar absorption patterns in range of 600–900 nm can be observed in three neat films, with the maximum absorption peak at 809 nm for D1, 801 nm for D2, and 783 nm for D3. The optical bandgaps (E_g^{opt}) could be roughly estimated through the thin-film absorption edge, being 1.38, 1.43, and 1.45 eV for D1, D2, and D3, respectively (Table S2, Supporting Information). The gradually enlarged bandgaps from D1 to D3 agrees well with the obtained results from both DFT calculation and CV. Compared with D3 whose substituent is electron-withdrawing group of —CF_3, D1 and D2 that are featured with electron-donating —OCH_3 and —CH_3 substituents, possess the obviously redshifted absorptions. This has demonstrated the great potential to conduct bandgap engineering of dimeric acceptors by means of central substituent tuning. It is also worth noting that D2 possesses the sharpest absorption edge comparing to other two counterparts in the low energy region (proved by the slopes of −0.012, −0.017, and −0.015 for D1, D2, and D3, respectively), suggesting the more ordered intermolecular stacking and lower energy disorder in D2 films (Figure S5, Supporting Information).[46,47]

Generally speaking, the unique geometry of 3D molecule may play a crucially important or even determining role in molecular packing, thus further affecting exciton separation, charge transport, and photovoltaic performance in resulting OSCs.[48] Therefore, we performed grazing incidence wide-angle X-ray scattering (GIWAXS) to shed light on the different molecular packing behaviors of D1, D2, and D3.[49] As displayed in Figures S6–S7 of the Supporting Information, all the three dimeric acceptors exhibited (010) diffraction peaks at 1.60 $Å^{-1}$ for D1, 1.58 $Å^{-1}$ for D2, and 1.56 $Å^{-1}$ for D3 in out-of-plane (OOP) directions and the similar (100) diffraction peaks locating at 0.28 $Å^{-1}$ in in-plane (IP) directions. The slightly enlarged π–π stacking distances (≈3.93 Å for D1, ≈3.97 for D2, and ≈4.03 Å for D3) were observed from D1 to D3, which are mainly caused by the increase of steric hindrance. However, the interlayer distances for D2 and D3 (≈22.4 Å) are slightly smaller than that of D1 (≈23.3 Å), suggesting the formation of more robust packing network and enhanced noncovalent interactions between adjacent layers for D2 and D3.[50] Moreover, the slightly larger crystal coherence lengths (CCLs) for D2 (21.74 Å) can also be observed with respect to that of D1 (18.84 Å) and D3 (20.93 Å), indicating more ordered molecular packings in D2 aggregates. This agrees well with the sharpest absorption edge for D2 among the three dimeric acceptors (Figure S5, Supporting Information). Generally, the more ordered molecular stacking in D2 aggerate will lead to more favorable charge transport/collection processes, thus possibly resulting in the improved FFs and J_{SC}s in OSCs.[51] The detailed parameters of π–π packing distances and CCLs that could reflect molecular packing features, have been illustrated in Table S3 of the Supporting Information for a clear comparison.

The photovoltaic property variation caused by central substituents was further evaluated by fabricating OSCs with a device structure of ITO/PEDOT:PSS/PM6:dimeric acceptor/PNDIT-F3N/Ag. Due to the complementary absorption and suitable energy levels, high-performance PM6 was selected as the polymeric donor to blend with dimeric acceptors studied here (Figure S8, Supporting Information).[52] The data of device optimization were presented in Tables S4–S6 of the Supporting Information, and the best current density–voltage (J–V) curves were shown in **Figure 2a**. Benefiting from the desirable features of D2 at both single molecular and aggregated levels, PM6:D2-based OSC afforded a champion PCE of 17.50% along with overall improved V_{OC} of 0.926 V, FF of 75.50%, and J_{SC} of 25.02 mA cm^{-2} comparing to those of other two counterparts (**Table 1**). It is noticed that PM6:D2-based OSCs show the best V_{OC} of 0.926 V among three systems. This is consistent with the data of electroluminescence external quantum efficiency (EQE_{EL}). As shown in Figure S9 and Table S7 of the Supporting Information, the higher EQE_{EL} for PM6:D2 could be observed, leading to the lower non-radiative energy loss (ΔV_{nr}) of 0.194 V comparing to that of 0.211 V for PM6:D1 and 0.228 V for PM6:D3. The best V_{OC} for PM6:D2-based devices might benefit from the lower nonradiative energy loss.

As recorded in Figure 2b, the integrated J_{SC}s calculated from EQE plots match well with the values derived from J–V tests. Note that EQEs and FFs of PM6:D2-based OSCs are much larger than those of PM6:D1-based one. This may be attributed to the more ordered molecular stacking of D2 and further the facilitated charge generation/transport dynamics in PM6:D2-blended films.

It is notable that the similar EQE values could be obtained by both PM6:D2 and PM6:D3 based OSCs when excluding the interference of different absorption range. However, an obviously lower EQE for PM6:D1 has been observed comparing to that of PM6:D2 and PM6:D3. As known to all, EQEs are determined by numerous factors, such as light harvesting capacity, charge generation/transport/recombination dynamics, etc., in active layers.[53] The PM6:D2 blend showed the enhanced absorption in acceptor

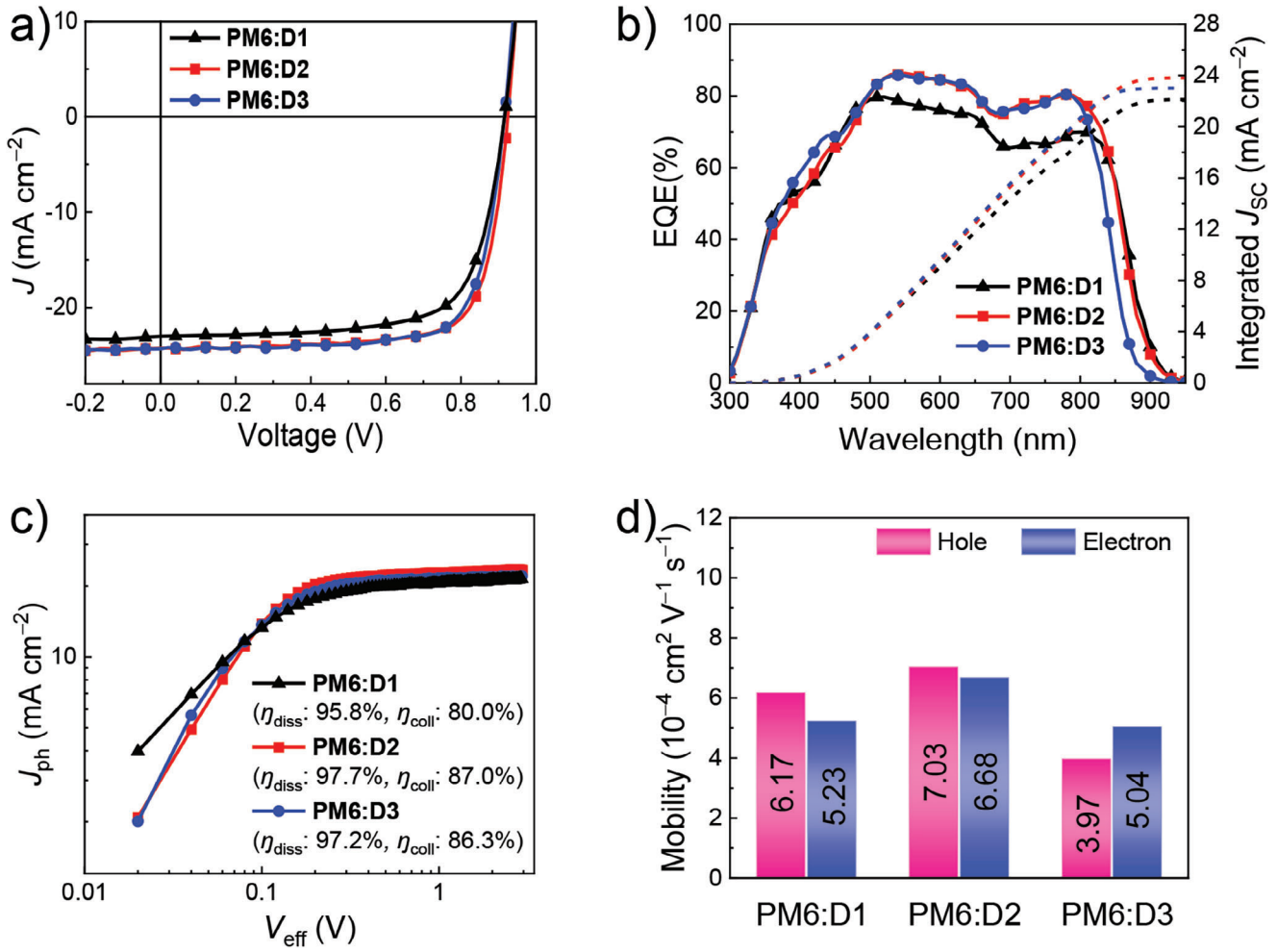

Figure 2. a) *J–V* curves of OSCs based on PM6:D1, PM6:D2, and PM6:D3 blends. b) EQE plots of OSCs based on PM6:D1, PM6:D2, and PM6:D3 blends. c) Plots of J_{ph} versus V_{eff}. The efficiencies of charge generation and collection were also provided. d) Hole and electron mobilities of PM6:D1, PM6:D2, and PM6:D3 blends.

Table 1. Summary of photovoltaic parameters for OSCs.

Active layers[a)]	V_{OC} [V]	J_{SC} [mA cm^{-2}]	Cal. J_{SC}[b)] [mA cm^{-2}]	FF [%]	PCE [%]
PM6:D1	0.916	23.03	22.37	71.24	15.04
	(0.917 ± 0.002)	(22.87±0.31)		(70.52 ± 0.90)	(14.78 ± 0.16)
PM6:D2	0.926	25.02	24.10	75.50	17.50
	(0.929 ± 0.004)	(24.66 ± 0.31)		(75.16 ± 0.36)	(17.22 ± 0.19)
PM6:D3	0.919	24.21	23.33	74.63	16.60
	(0.910 ± 0.008)	(24.09 ± 0.33)		(74.98 ± 0.75)	(16.43 ± 0.22)

[a)] Average parameters derived from 15 independent OSCs (Tables S8–S10, Supporting Information) [b)] Current densities by integrating EQE plots.

region comparing to PM6:D1 and PM6:D3 blends (Figure S10, Supporting Information), which will also contribute to the better EQE response of D2-based OSCs. Besides, with the aim of further shedding light on the EQE variation (employing PM6:D1 and PM6:D2 for a simplified discussion here), exciton dissociation efficiency (P_{diss}) and charge collection efficiency (P_{coll}) were evaluated by measuring the dependence of photocurrent density (J_{ph}) versus effective voltage (V_{eff}).[54] As displayed in Figure 2c, J_{ph} can quickly approach saturation with V_{eff} increasing, indicating an efficient process of exciton dissociation. As a result, D1 and D2 based devices afforded the corresponding exciton dissociation efficiencies (η_{diss}) of 95.8% and 97.7%, respectively. Meanwhile, the charge collection efficiencies (η_{coll}) can also be calculated to be 80.0% for D1 and 87.0% for D2-based OSCs. The

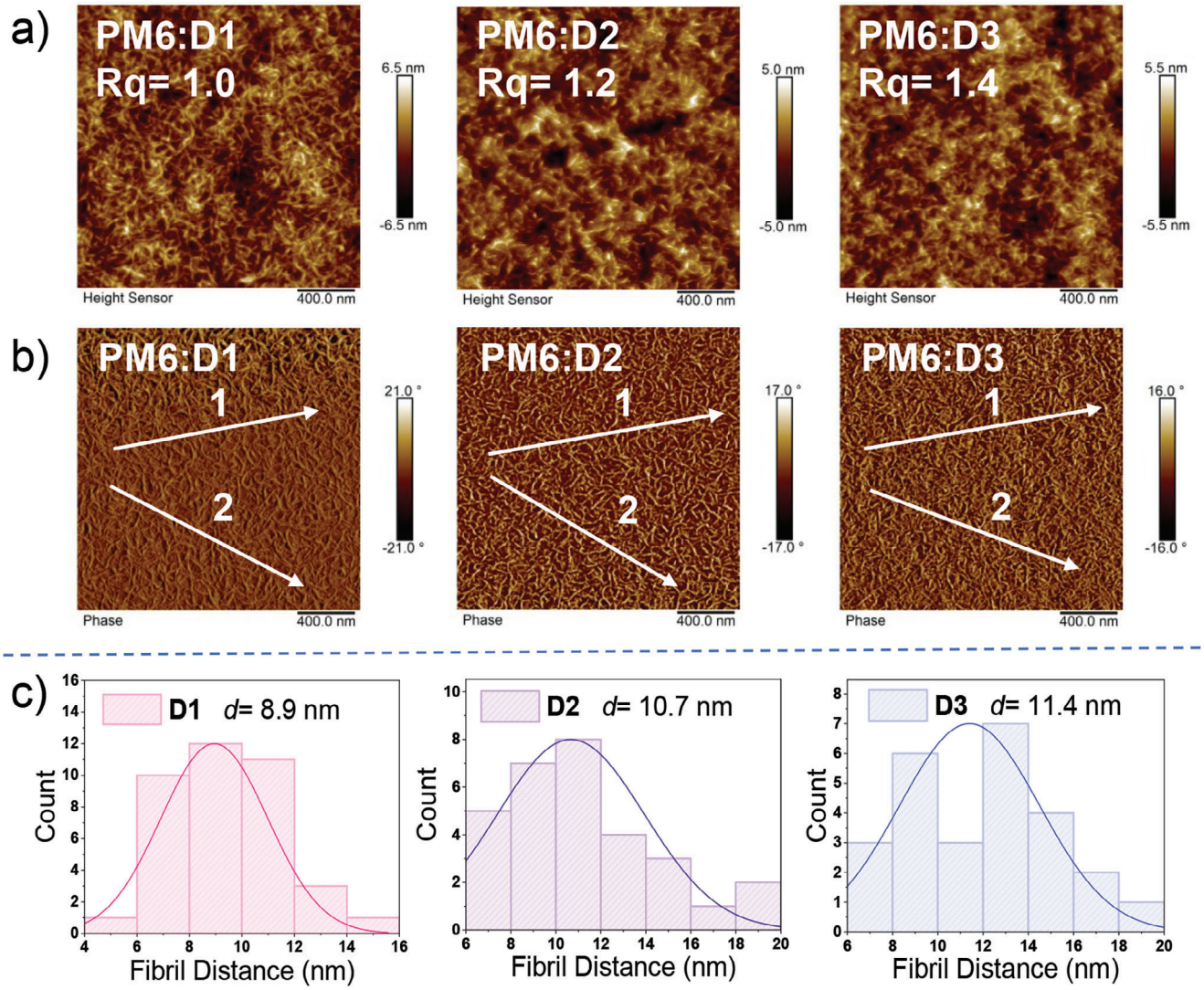

Figure 3. a) AFM height images of blended films. b) AFM phase images of blended films. c) Statistical distribution of fibril diameters.

improved exciton dissociation and charge collection for D2-based devices should mainly account for its larger EQE values comparing to that of D1.

Note that the energy offset at D/A interfaces, which is usually regarded as the driving force for exciton dissociation, is closely related to the η_{diss}. Comparing to D1, D2 possesses the downshifted HOMO energy levels, thus giving rise to an increased driving force for charge generation. Thereby it is reasonable to find a slightly larger η_{diss} for D2-based devices. On the other hand, the improved η_{coll} of PM6:D2 may be determined by their ordered molecular packing and optimized film morphology comparing to that of PM6:D1 (discussed in detail below). The charge recombination behaviors in D1 and D2 based OSCs were also examined by recording the light intensity (P_{light}) dependence of J_{SC} and V_{OC} (Figure S11, Supporting Information).[55] The similar but negligible bimolecular/trap-assisted recombination could be observed, indicated by the derived slopes that close to unit.[56] This agrees well with the similar transient photovoltage decay kinetics of D1 and D2 based devices (Figure S12, Supporting Information), charge carrier lifetime: 96 µs for PM6:D1; 97 µs for PM6:D2). In addition, the charge extraction time of PM6:D2-based device (0.41 µs) was slightly smaller than that of PM6:D1-based device (0.65 µs), suggesting the faster charge transporting in PM6:D2-based OSCs. Therefore, we further employed the space-charge limited current method to monitor the carrier transport features of D1, D2, and D3 films. Figure 2d illustrated the hole (μ_h)/electron (μ_e) mobilities of two systems, being $6.17 \times 10^{-4}/5.23 \times 10^{-4}$ cm^2 V^{-1} s^{-1} for PM6:D1 and $7.03 \times 10^{-4}/6.68 \times 10^{-4}$ cm^2 V^{-1} s^{-1} for PM6:D2, respectively. Moreover, the pure film of D2 also showed a higher charge mobility comparing to that of D1. Therefore, the slightly improved mobilities for D2 along with more balanced μ_e/μ_h ratio (1.05 for D2 and 1.18 for D1) in blended films should be responsible for the larger EQEs and FFs than that of D1-based OSCs (Figure S13 and Table S11, Supporting Information).

The improved photovoltaic performance of D2-based OSCs should be closely correlate with its better nanoscale morphology in D/A blended films.[57,58] Therefore, we employed atomic

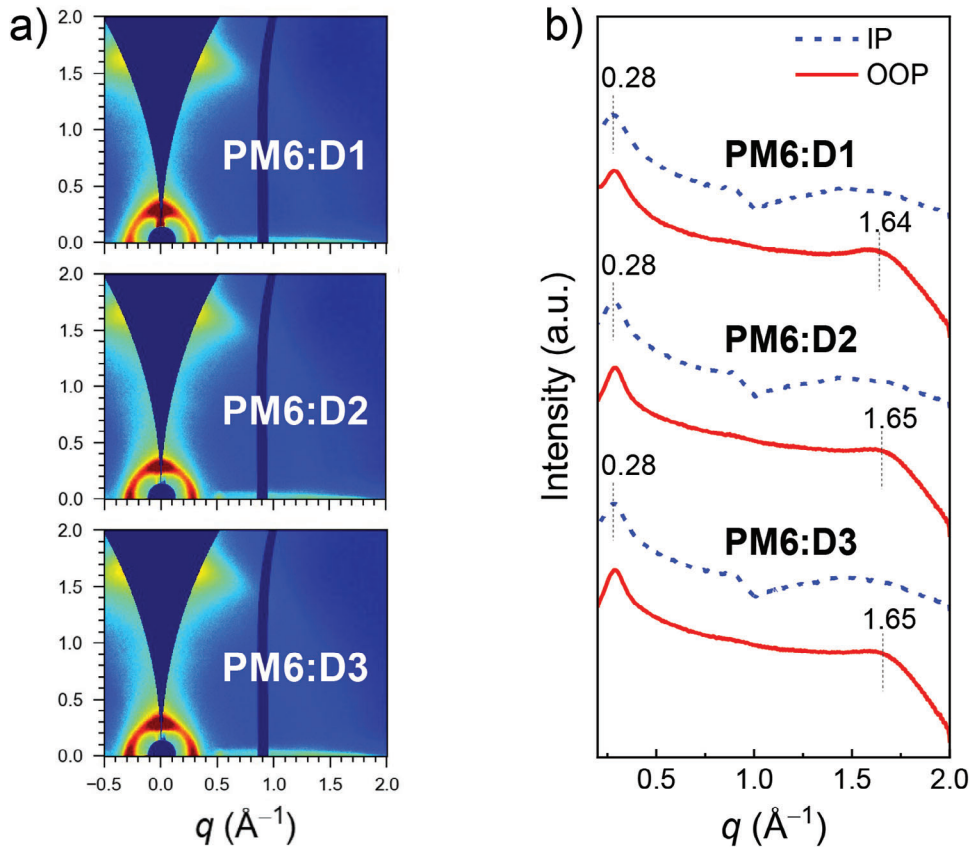

Figure 4. a) 2D GIWAXS patterns of blended films. b) Extracted line-cut profiles from 2D GIWAXS patterns of blended films.

force microscopy (AFM) to unveil the film morphology differences. Generally, all the three blended films displayed appropriate phase separations (**Figure 3**a,b), but gradually enlarged surface root-mean-square roughness values (1.0 nm for PM6:D1, 1.2 nm for PM6:D2, and 1.4 nm for PM6:D3). By further carrying out a statistical analysis of nanofiber size, a stepwise enlarged fiber size could be estimated as 8.9, 10.7, and 11.4 nm for PM6:D1, PM6:D2, and PM6:D3, respectively (Figure 3c; Figure S14, Supporting Information). These results imply the improved molecular crystallinity of D2 and D3 comparing to that of D1. In addition, the $\chi_{D:A}$, which could reflect the miscibility between donor and acceptor materials, increased from D1 to D3 (Figure S15 and Table S12, Supporting Information), implying the decreased D/A miscibility from PM6:D1 to PM6:D3.[59] This may be caused the different dihedral angles that affect the π–π stacking of conjugated backbones between dimeric acceptors and PM6, and should account for the enlarged fiber size in blended films from PM6:D1 to PM6:D3. In light of the great effects of molecular stacking on obtaining the superior photodynamics in OSCs, GIWAXS analysis of blended films was further carried out. All the blended films exhibited the similar π–π stacking (010) diffraction peaks at 1.65 $Å^{-1}$ in OOP direction and (100) diffraction peaks at 0.28 $Å^{-1}$ in IP direction (**Figure 4**a,b). Similar to neat films of acceptors, the slightly larger CCLs (21.74 Å) for PM6:D2 and PM6:D3 can also be observed with respect to that of 20.93 Å for PM6:D1, indicating the improved crystalline ordering of D2 and D3 could be maintained in resulting blended films (Table S13, Supporting Information). To sum up, the suitable size of nanofibers and improved crystalline ordering in PM6:D2 and PM6:D3 blends should account for their facilitated charge separation/transport and better photovoltaic performance.[60,61] It is worth noting that the crucial role of central substituents in morphology control has been fully proved, thus providing a feasible pathway to optimize photovoltaic performance of dimeric acceptors by introducing proper central substituents rationally.

Apart from the efficiency of OSCs, the desirable morphological stability toward excellent device stability is also crucially important for the large-scale application of OSCs.[62,63] Therefore, the storage stability of these dimeric acceptor-based OSCs as well as their thermal stability were further evaluated. As depicted in **Figure 5**a, all the devices maintained over 90% of their initial PCEs after 2000 h, exhibiting the excellent storage stability. By exerting thermal stress on OSCs at 65 °C in a nitrogen-filled glovebox, the PCEs of OSCs based on PM6:D1 and PM6:D2 decreased with the aging time increasing, but still kept ≈80% of their original PCEs after 600 h. However, the PCE of D3-based OSCs suffered from a fast decay and dropped below 70% under the same aging condition after 200 h (Figure 5b). To gain a deeper insight into the time dependent PCE evolution, atomic force microscopy-infrared absorption spectroscopy (AFM-IR) was conducted to monitor the phase separation before and after thermal aging. As presented in Figure 5c, the desirable D/A interpenetrating networks at nanoscale could be achieved by all the three systems. Among them, PM6:D2-based blend seems to exhibit the

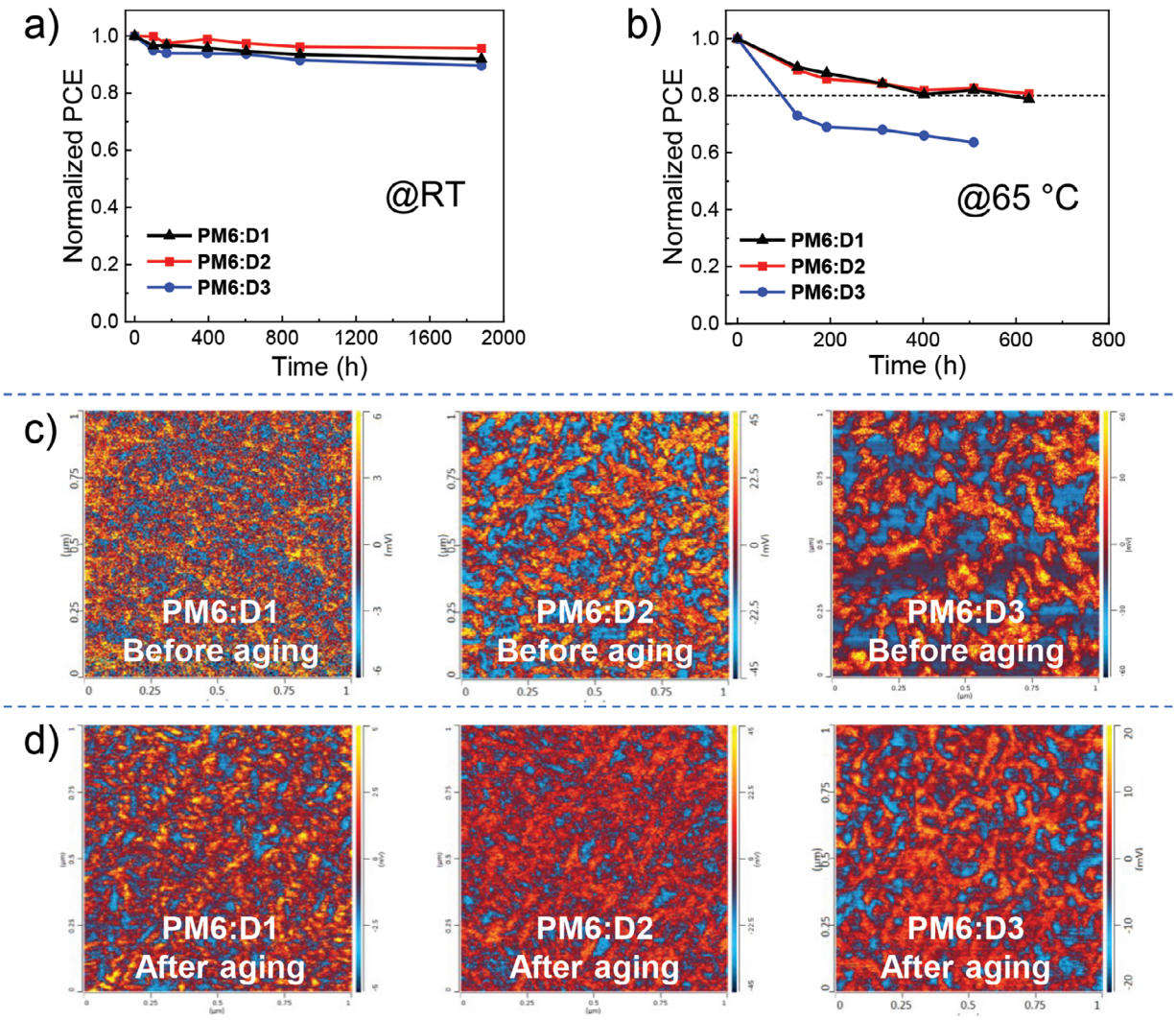

Figure 5. a) Storage stability and b) thermal stability of optimal devices. c) AFM-IR images of blended films without heat aging. d) AFM-IR images of blended films after heat aging at 65 °C for a week.

more consecutive nanofiber network and appropriate phase separation, which are supposed to be the key factor of its efficient charge transportation and extraction.[64,65] After thermal aging for a week, all the three blends still maintained the desirable D/A interpenetrating networks, however, the phase separation size enlarged greatly (Figure 5d). Especially for PM6:D3 blend, the markedly oversize D/A phases emerged, which should account for the dramatic PCE decrease of OSCs. Note that this dramatic morphology evolution of PM6:D3 blend after thermal aging should be ascribed to the relatively strong crystallinity of D3, which is induced by the central substituents of trifluoromethyl group.

3. Conclusion

In order to explore the effect of central substituents on molecular configuration/stacking and photovoltaic performance, a series of dimeric acceptors were constructed on basis of the same 3D conjugated molecular skeleton but with diverse substituents (—OCH_3 for D1, —CH_3 for D2, and —CF_3 for D3) grafting on central units. The introduction of —OCH_3 leads to the smallest dihedral angle between two monomer-like conjugated planes, owing to the formation of noncovalently conformational locks through O–S interactions. When replacing —OCH_3 with —CH_3 and —CF_3, the dihedral angles increase greatly. Due to the enlarged dihedral angles of D2 and D3, a more robust packing network with enhanced noncovalent interactions between adjacent layers was achieved. Moreover, not only does the molecular conformation change significantly, but also the absorption spectra blueshifted gradually as the electron-donating ability of central substituents weakens. When further blending dimeric acceptors with PM6 donor, the desirable D/A interpenetrating networks at nanoscale could be achieved by all the three systems. Among them, PM6:D2-based blend seems to exhibit the more consecutive nanofiber network and appropriate phase separation due to the improved crystalline ordering of D2 and suitable miscibility with PM6 donor. As a consequence, benefitting from the facilitated exciton dissociation and charge collection, OSCs based on

PM6:D2 achieve an excellent PCE of 17.50% along with a good long-term stability. An inner morphology investigation has revealed that the markedly oversize D/A phase separation emerged after thermal aging, especially for PM6:D3 blend, in spite of the remaining D/A interpenetrating networks. This should account for the unsatisfied thermal stability for all the three OSCs. Such a success in dimeric molecular design highlights the effectiveness of central substituents in structure optimization and provides a feasible pathway to construct much more efficient dimeric acceptors through central substituent regulation.

Supporting Information

Supporting Information is available from the Wiley Online Library or from the author.

Acknowledgements

The authors gratefully acknowledge the financial support from Ministry of Science and Technology of the People's Republic of China (National Key R&D Program of China (2022YFB4200400, 2019YFA0705900, and 2023YFE0210400) and National Natural Science Foundation of China (22204119, 21935007, 52025033, 22361132530, and 22309090). The authors gratefully acknowledge the cooperation of the beamline scientists at BSRF-1W1A beamline (Beijing).

Conflict of Interest

The authors declare no conflict of interest.

Author Contributions

X.J. and Y.L. contributed equally to this work. The synthetic works were carried out by Y.L. The device optimizations, measurements, and original manuscript were carried out by X.J. X.C. and X.B. helped to analyze the data. W.Z. performed the DFT calculations. Z.Y. and Y.C. conceived and directed the study and review the manuscript. G.L., B.K., C.L., X.W., and Y.C. helped to analyze the data and commented on the manuscript.

Data Availability Statement

The data that support the findings of this study are available from the corresponding author upon reasonable request.

Keywords

central substitution, dimeric acceptors, morphology regulation, organic solar cells

Received: July 15, 2024
Revised: August 27, 2024
Published online:

[1] L. X. Chen, *ACS Energy Lett.* **2019**, *4*, 2537.
[2] C. W. Tang, *Appl. Phys. Lett.* **1986**, *48*, 183.
[3] G. Yu, J. Gao, J. C. Hummelen, F. Wudl, A. J. Heeger, *Science* **1995**, *270*, 1789.
[4] X. Zheng, L. Zuo, F. Zhao, Y. Li, T. Chen, S. Shan, K. Yan, Y. Pan, B. Xu, C.-Z. Li, M. Shi, J. Hou, H. Chen, *Adv. Mater.* **2022**, *34*, 2200044.
[5] P. Xue, P. Xue, P. Cheng, P. Cheng, R. P. S. Han, R. P. S. Han, X. Zhan, X. Zhan, *Mater. Horiz.* **2022**, *9*, 194.
[6] S. Dai, X. Zhan, *Adv. Energy Mater.* **2018**, *8*, 1800002.
[7] Y. Sun, L. Wang, C. Guo, J. Xiao, C. Liu, C. Chen, W. Xia, Z. Gan, J. Cheng, J. Zhou, Z. Chen, J. Zhou, D. Liu, T. Wang, W. Li, *J. Am. Chem. Soc.* **2024**, *146*, 12011.
[8] S. Guan, Y. Li, C. Xu, N. Yin, C. Xu, C. Wang, M. Wang, Y. Xu, Q. Chen, D. Wang, L. Zuo, H. Chen, *Adv. Mater.* **2024**, *36*, 2400342.
[9] P. Bi, J. Wang, Y. Cui, J. Zhang, T. Zhang, Z. Chen, J. Qiao, J. Dai, S. Zhang, X. Hao, Z. Wei, J. Hou, *Adv. Mater.* **2023**, *35*, 202210865.
[10] H. Lu, D. Li, W. Liu, G. Ran, H. Wu, N. Wei, Z. Tang, Y. Liu, W. Zhang, Z. Bo, *Angew. Chem., Int. Ed.* **2024**, *63*, 202407007.
[11] B. Pang, C. Liao, X. Xu, L. Yu, R. Li, Q. Peng, *Adv. Mater.* **2023**, *35*, 2300631.
[12] R. Zeng, S. Xu, J. Deng, S. Tan, G. Zhou, M. Zhang, L. Zhu, F. Han, X. Xue, A. Zhang, H. Tan, L. Zhang, C. Zhu, C. Wang, X. Wu, Z. Fink, T. P. Russell, Y. Zhang, F. Liu, *Adv. Energy Mater.* **2024**, 2401561.
[13] H. Fu, J. Yao, M. Zhang, L. Xue, Q. Zhou, S. Li, M. Lei, L. Meng, Z.-G. Zhang, Y. Li, *Nat. Commun.* **2022**, *13*, 3687.
[14] C. Wang, X. Ma, Y. Shen, D. Deng, H. Zhang, T. Wang, J. Zhang, J. Li, R. Wang, L. Zhang, Q. Cheng, Z. Zhang, H. Zhou, C. Tian, Z. Wei, *Joule* **2023**, *7*, 2386.
[15] M. Lv, Q. Wang, J. Zhang, Y. Wang, Z.-G. Zhang, T. Wang, H. Zhang, K. Lu, Z. Wei, D. Deng, *Adv. Mater.* **2024**, *36*, 2310046.
[16] H. Yu, Y. Wang, H. K. Kim, X. Wu, Y. Li, Z. Yao, M. Pan, X. Zou, J. Zhang, S. Chen, D. Zhao, F. Huang, X. Lu, Z. Zhu, H. Yan, *Adv. Mater.* **2022**, *34*, 2200361.
[17] J.-W. Lee, J.-W. Lee, C. Sun, C. Sun, T. N.-L. Phan, T. N.-L. Phan, D. C. Lee, D. C. Lee, Z. Tan, Z. Tan, H. Jeon, H. Jeon, S. Cho, S. Cho, S.-K. Kwon, S.-K. Kwon, Y.-H. Kim, Y.-H. Kim, B. J. Kim, B. J. Kim, *Energy Environ. Sci.* **2023**, *16*, 3339.
[18] K. Ma, H. Liang, Y. Wang, Z. Xiao, C. Jiang, W. Feng, Z. Zhang, X. Si, J. Liu, X. Wan, B. Kan, C. Li, Z. Yao, Y. Chen, *ACS Mater. Lett.* **2023**, *5*, 884.
[19] Y. Liang, D. Zhang, Z. Wu, T. Jia, L. Lüer, H. Tang, L. Hong, J. Zhang, K. Zhang, C. J. Brabec, N. Li, F. Huang, *Nat. Energy* **2022**, *7*, 1180.
[20] H. Zhuo, X. Li, J. Zhang, S. Qin, J. Guo, R. Zhou, X. Jiang, X. Wu, Z. Chen, J. Li, L. Meng, Y. Li, *Angew. Chem., Int. Ed.* **2023**, *62*, 202303551.
[21] F. Qi, Y. Li, R. Zhang, F. R. Lin, K. Liu, Q. Fan, A. K. Y. Jen, *Angew. Chem., Int. Ed.* **2023**, *62*, 202303066.
[22] G. Sun, X. Jiang, X. Li, L. Meng, J. Zhang, S. Qin, X. Kong, J. Li, J. Xin, W. Ma, Y. Li, *Nat. Commun.* **2022**, *13*, 5267.
[23] H. Wang, C. Cao, H. Chen, H. Lai, C. Ke, Y. Zhu, H. Li, F. He, *Angew. Chem., Int. Ed.* **2022**, *61*, 202201844.
[24] X. Gu, X. Zhang, H. Huang, *Angew. Chem., Int. Ed.* **2023**, *62*, 202308496.
[25] H. Chen, Y. Zou, H. Liang, T. He, X. Xu, Y. Zhang, Z. Ma, J. Wang, M. Zhang, Q. Li, C. Li, G. Long, X. Wan, Z. Yao, Y. Chen, *Sci. China: Chem.* **2022**, *65*, 1362.
[26] W. Zhu, A. P. Spencer, S. Mukherjee, J. M. Alzola, V. K. Sangwan, S. H. Amsterdam, S. M. Swick, L. O. Jones, M. C. Heiber, A. A. Herzing, G. Li, C. L. Stern, D. M. DeLongchamp, K. L. Kohlstedt, M. C. Hersam, G. C. Schatz, M. R. Wasielewski, L. X. Chen, A. Facchetti, T. J. Marks, *J. Am. Chem. Soc.* **2020**, *142*, 14532.
[27] J. Cao, L. Yi, L. Ding, J. Cao, L. Yi, L. Ding, *J. Semicond.* **2022**, *43*, 030202.
[28] X. Gu, Y. Wei, N. Yu, J. Qiao, Z. Han, Q. Lin, X. Han, J. Gao, C. Li, J. Zhang, X. Hao, Z. Wei, Z. Tang, Y. Cai, X. Zhang, H. Huang, *CCS Chem.* **2023**, *5*, 2576.
[29] W. Wei, X. Zhou, S. Pang, J. Zhou, X. Yuan, J. Li, Y. Chen, L. Pan, Z. Xie, H. Wu, F. Huang, Y. Cao, C. Duan, *Aggregate* **2024**, *5*, 488.

[30] T.-J. Wen, Z.-X. Liu, Z. Chen, J. Zhou, Z. Shen, Y. Xiao, X. Lu, Z. Xie, H. Zhu, C.-Z. Li, H. Chen, *Angew. Chem., Int. Ed.* **2021**, *60*, 12964.
[31] T. J. Aldrich, M. Matta, W. Zhu, S. M. Swick, C. L. Stern, G. C. Schatz, A. Facchetti, F. S. Melkonyan, T. J. Marks, *J. Am. Chem. Soc.* **2019**, *141*, 3274.
[32] S. Wan, Y. Ma, D. Cai, W. Lin, P. Wang, J. Wang, Q. Zheng, *Adv. Funct. Mater.* **2021**, *31*, 2010436.
[33] C. He, Z. Chen, T. Wang, Z. Shen, Y. Li, J. Zhou, J. Yu, H. Fang, Y. Li, S. Li, X. Lu, W. Ma, F. Gao, Z. Xie, V. Coropceanu, H. Zhu, J.-L. Bredas, L. Zuo, H. Chen, *Nat. Commun.* **2022**, *13*, 2598.
[34] F. Liu, T. Hou, X. Xu, L. Sun, J. Zhou, X. Zhao, S. Zhang, *Macromol. Rapid Commun.* **2018**, *39*, 1700555.
[35] H. Chen, X. Cao, X. Xu, C. Li, X. Wan, Z. Yao, Y. Chen, H. Chen, X. Cao, X. Xu, C. Li, X. Wan, Z. Yao, Y. Chen, *Chin. J. Polym. Sci.* **2022**, *40*, 921.
[36] X. Meng, M. Li, K. Jin, L. Zhang, J. Sun, W. Zhang, C. Yi, J. Yang, F. Hao, G.-W. Wang, Z. Xiao, L. Ding, *Angew. Chem., Int. Ed.* **2022**, *61*, 202207762.
[37] H. Chen, Z. Zhang, P. Wang, Y. Zhang, K. Ma, Y. Lin, T. Duan, T. He, Z. Ma, G. Long, C. Li, B. Kan, Z. Yao, X. Wan, Y. Chen, *Energy Environ. Sci.* **2023**, *16*, 1773.
[38] H. Chen, B. Kan, P. Wang, W. Feng, L. Li, S. Zhang, T. Chen, Y. Yang, T. Duan, Z. Yao, C. Li, X. Wan, Y. Chen, *Angew. Chem., Int. Ed.* **2023**, *62*, 202307962.
[39] F. Yi, M. Xiao, Y. Meng, H. Bai, W. Su, W. Gao, Z.-F. Yao, G. Qi, Z. Liang, C. Jin, L. Tang, R. Zhang, L. Yan, Y. Liu, W. Zhu, W. Ma, Q. Fan, *Angew. Chem., Int. Ed.* **2024**, *63*, 202319295.
[40] Z. Yao, X. Cao, X. Bi, T. He, Y. Li, X. Jia, H. Liang, Y. Guo, G. Long, B. Kan, C. Li, X. Wan, Y. Chen, *Angew. Chem., Int. Ed.* **2023**, *62*, 202312630.
[41] H. Liang, X. Bi, H. Chen, T. He, Y. Lin, Y. Zhang, K. Ma, W. Feng, Z. Ma, G. Long, C. Li, B. Kan, H. Zhang, O. A. Rakitin, X. Wan, Z. Yao, Y. Chen, *Nat. Commun.* **2023**, *14*, 4707.
[42] Y. Li, F. Qi, B. Fan, K.-K. Liu, J. Yu, Y. Fu, X. Liu, Z. Wang, S. Zhang, G. Lu, X. Lu, Q. Fan, P. C. Y. Chow, W. Ma, F. R. Lin, A. K.-Y. Jen, *Adv. Mater.* **2024**, *36*, 2313393.
[43] S. Yu, A. Peng, S. Zhang, H. Huang, *Sci. China: Chem.* **2018**, *61*, 1359.
[44] W. Wei, C. e. Zhang, Z. Chen, W. Chen, G. Ran, G. Pan, W. Zhang, P. Müller-Buschbaum, Z. Bo, C. Yang, Z. Luo, *Angew. Chem., Int. Ed.* **2024**, *63*, 202315625.
[45] Y. Cui, P. Zhu, X. Liao, Y. Chen, *J. Mater. Chem. C* **2020**, *8*, 15920.
[46] Z. Zhang, Y. Li, G. Cai, Y. Zhang, X. Lu, Y. Lin, *J. Am. Chem. Soc.* **2020**, *142*, 18741.
[47] S. Liu, J. Yuan, W. Deng, M. Luo, Y. Xie, Q. Liang, Y. Zou, Z. He, H. Wu, Y. Cao, *Nat. Photonics* **2020**, *14*, 300.
[48] D. Meng, J. L. Yang, C. Xiao, R. Wang, X. Xing, O. Kocak, G. Aydin, I. Yavuz, S. Nuryyeva, L. Zhang, G. Liu, Z. Li, S. Yuan, Z.-K. Wang, W. Wei, Z. Wang, K. N. Houk, Y. Yang, D. Meng, J. L. Yang, C. Xiao, R. Wang, X. Xing, O. Kocak, G. Aydin, I. Yavuz, S. Nuryyeva, L. Zhang, G. Liu, Z. Li, et al., *Proc. Natl. Acad. Sci. USA* **2020**, *117*, 2010733117.
[49] P. Müller-Buschbaum, *Adv. Mater.* **2014**, *26*, 7692.
[50] Q. Shen, C. He, S. Li, L. Zuo, M. Shi, H. Chen, *Acc. Mater. Res.* **2022**, *3*, 644.
[51] X. Zhang, C. Li, J. Xu, R. Wang, J. Song, H. Zhang, Y. Li, Y.-N. Jing, S. Li, G. Wu, J. Zhou, X. Li, Y. Zhang, X. Li, J. Zhang, C. Zhang, H. Zhou, Y. Sun, Y. Zhang, *Joule* **2022**, *6*, 444.
[52] M. Zhang, X. Guo, W. Ma, H. Ade, J. Hou, *Adv. Mater.* **2015**, *27*, 4655.
[53] X.-K. Chen, V. Coropceanu, J.-L. Brédas, *Nat. Commun.* **2018**, *9*, 5295.
[54] A. K. K. Kyaw, D. H. Wang, V. Gupta, W. L. Leong, L. Ke, G. C. Bazan, A. J. Heeger, *ACS Nano* **2013**, *7*, 4569.
[55] G. Liu, R. Xia, Q. Huang, K. Zhang, Z. Hu, T. Jia, X. Liu, H.-L. Yip, F. Huang, *Adv. Funct. Mater.* **2021**, *31*, 2103283.
[56] L. J. A. Koster, V. D. Mihailetchi, R. Ramaker, P. W. M. Blom, *Appl. Phys. Lett.* **2005**, *86*, 123509.
[57] Y. Huang, E. J. Kramer, A. J. Heeger, G. C. Bazan, *Chem. Rev.* **2014**, *114*, 7006.
[58] T. Wang, X.-K. Chen, A. Ashokan, Z. Zheng, M. K. Ravva, J.-L. Brédas, *Adv. Funct. Mater.* **2018**, *28*, 1705868.
[59] L. Ye, B. A. Collins, X. Jiao, J. Zhao, H. Yan, H. Ade, *Adv. Energy Mater.* **2018**, *8*, 1703058.
[60] Q. Liu, Y. Jiang, K. Jin, J. Qin, J. Xu, W. Li, J. Xiong, J. Liu, Z. Xiao, K. Sun, S. Yang, X. Zhang, L. Ding, *Sci. Bull.* **2020**, *65*, 272.
[61] T. Xu, Z. Luo, R. Ma, Z. Chen, T. A. Dela Peña, H. Liu, Q. Wei, M. Li, C. E. Zhang, J. Wu, X. Lu, G. Li, C. Yang, *Angew. Chem., Int. Ed.* **2023**, *62*, 202304127.
[62] S. Li, R. Zhang, M. Zhang, J. Yao, Z. Peng, Q. Chen, C. Zhang, B. Chang, Y. Bai, H. Fu, Y. Ouyang, C. Zhang, J. A. Steele, T. Alshahrani, M. B. J. Roeffaers, E. Solano, L. Meng, F. Gao, Y. Li, Z.-G. Zhang, *Adv. Mater.* **2023**, *35*, 2206563.
[63] Y. Li, X. Huang, K. Ding, H. K. M. Sheriff, L. Ye, H. Liu, C.-Z. Li, H. Ade, S. R. Forrest, *Nat. Commun.* **2021**, *12*, 5419.
[64] S. Nilsson, A. Bernasik, A. Budkowski, E. Moons, *Macromolecules* **2007**, *40*, 8291.
[65] X. He, Z.-X. Liu, H. Chen, C.-Z. Li, *Adv. Mater.* **2024**, *36*, 2306681.